INSTITUTE OF PHYSICS PUBLISHING JOURNAL OF PHYSICS: CONDENSED MATTER

J. Phys.: Condens. Matter **14** (2002) 5979–6004 PII: S0953-8984(02)37443-5

Dynamical fluctuations and the $\sqrt{3} \times \sqrt{3} \leftrightarrow 3 \times 3$ transition in α-Sn/Ge(111) and Sn/Si(111)

José Ortega, Rubén Pérez and Fernando Flores

Departamento de Física Teórica de la Materia Condensada, Universidad Autónoma de Madrid, E-28049 Madrid, Spain

Received 27 May 2002
Published 31 May 2002
Online at stacks.iop.org/JPhysCM/14/5979

Abstract

A critical review of our understanding of the reversible phase transition $\sqrt{3} \times \sqrt{3} \leftrightarrow 3 \times 3$ for the α-phase of the Sn/Ge(111) and Sn/Si(111) interfaces is presented. Experimental data and theoretical calculations suggest the following. (a) Sn/Ge(111) presents a reversible phase transition associated with the freezing of a surface soft phonon. At high temperature the dynamical fluctuations of the underlying 3×3 structure give rise to the observed $\sqrt{3} \times \sqrt{3}$ symmetry. (b) Sn/Si(111) does not present the 3×3 phase although the $\sqrt{3} \times \sqrt{3}$ reconstruction should be understood within the dynamical fluctuations model found for Sn/Ge(111). (c) These properties are modulated, but not substantially modified, by either defects or by electron many-body effects. We discuss these two cases and analyse how they affect the surface geometry and the electronic properties of the system.

(Some figures in this article are in colour only in the electronic version)

1. Introduction

Adsorption systems such as Pb or Sn on Ge(111) and Si(111) have been for many years the workhorse of surface science. Due to the chemical similarity between adsorbate and substrate (they belong to group IV in the periodic table) these systems present atomically abrupt interfaces, and have been intensively studied since the beginning of the 1980s in an effort to understand the properties of Schottky contacts [1–3]. For example, the dependence of the Schottky barrier on the surface reconstruction, i.e. on the chemical bonds that form the adsorbate and substrate, was first demonstrated for the Pb/Si(111) system [4, 5]. On the other hand, these studies also exploit the variation in electronic properties (as a result of the competition between the promotion energy required to get an sp^3 hybridization and the strength of the fourth bond) as we move along the group: C is an insulator (or a semimetal in the graphite phase), Si and Ge are semiconductors, Sn is either a semiconductor (grey tin) or a metal (white tin), and finally Pb is a typical metal.

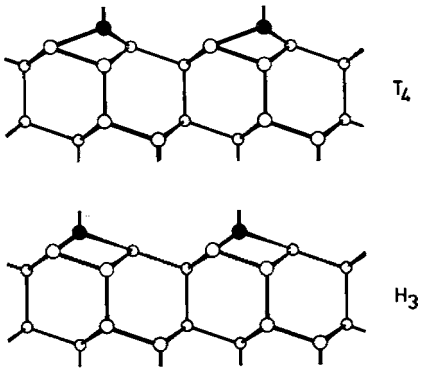

Figure 1. T_4 and H_4 sites for adsorption of adatoms (black circles) on (111) surfaces.

The phase diagrams of these systems, as a function of coverage and temperature, are quite complicated, with a large number of different reconstructions, the details depending on the nature of both adsorbate and substrate. In this work we shall concentrate on the submonolayer regime, and in particular on the $\sqrt{3}\times\sqrt{3}$R30° phase obtained for a 1/3 ML adsorbate coverage, the α-phase, that is common to the four interfaces Pb/Ge(111), Pb/Si(111), Sn/Ge(111), and Sn/Si(111).

Previous experience with other systems, such as group-III atoms on Si(111) [6], suggests that this reconstruction is stabilized by the reduction in the number of dangling bonds by adatom decoration: three dangling bonds of the ideal (111) surface are saturated by the interaction with each Pb or Sn adatom, leaving just the adatom dangling bond. This dangling bond is, in principle, occupied by one electron, giving rise to a half-occupied band crossing E_F. There are two threefold-symmetric positions on the surface that are compatible with this dangling-bond reduction (see figure 1): T_4 sites (adatom on top of the second Ge or Si layer), and H_4 hollow sites (adatom on top of the fourth Ge or Si layer). The determination of the structure of this phase in the Pb/Ge(111) system was one of the first applications of the x-ray diffraction [7] and x-ray standing-wave [8] methods developed in the late 1980s. These measurements indicate that Pb adatoms were absorbed in T_4 sites. Angle-resolved photoelectron spectroscopy (ARPES) measurements at the beginning of the 1990s [9, 10] further support the T_4 geometry and yield evidence of the metallicity of the surface. Theoretical calculations [11] later confirmed the T_4 position as the favourable adsorption site (-0.06 eV/atom below the H_4 position) and the presence of a half-occupied band, mainly associated with the p_z Pb dangling-bond orbital, although a significant weight is found in the p_z orbitals of the first- and second-layer Ge atoms.

After all this experimental and theoretical work, one might expect the α-$\sqrt{3}\times\sqrt{3}$ to be one of the best-understood reconstructions in surface science. However, there was already some contradictory evidence concerning such systems. Core-level photoemission spectroscopy (PES) [12] for the Sn 4d core level in Sn/Ge(111) and Sn/Si(111) shows unambiguously the presence of two different components in the line profile. From the T_4 model, one expects to find only one type of Sn atom on the surface and, as a consequence, one should only observe one component in the Sn 4d photoelectron spectra.

The recent interest in these systems arises from the observation in α-$\sqrt{3}\times\sqrt{3}$ Pb/Ge(111) of a reversible transition to a new 3×3 phase when the temperature was lowered below $-20\,^{\circ}$C [13]. This same phase transition was soon characterized in Sn/Ge(111) [14] and has also recently been observed in Pb/Si(111) [15, 16]. In contrast, no evidence of this transition has been found in Sn/Si(111) for temperatures as low as 38 K [15].

Since its discovery, different physical mechanisms have been proposed as the driving force underlying this phase transition: surface Fermi wavevector nesting or electron correlations leading to the formation of a surface charge-density wave (SCDW) at low temperature (LT) [13, 14, 17]; dynamical fluctuations of an underlying 3×3 structure—stabilized at LT by a soft phonon—and giving rise to the observation, on average, of a $\sqrt{3} \times \sqrt{3}$ symmetry at room temperature (RT) [18–21]; the interaction between the 3×3 periodicity and Ge substitutional defects that act as nucleation centres [22–24]; and, recently, a defect–defect interaction mediated by localized phonon modes [25].

In this work we show that the extensive experimental and theoretical work devoted to the characterization of this transition supports the role of dynamical fluctuations [18], frozen when the temperature is lowered, in the puzzling properties of all these systems. The experimental evidence is summarized in section 2, with particular attention given to the similarities of and differences between Sn/Ge(111) and Sn/Si(111). Sections 3 and 4 characterize the structural and electronic properties of the 3×3 phase, comparing theoretical and experimental results. The nature of the RT $\sqrt{3} \times \sqrt{3}$ phase and the reason that the transition is not observed in Sn/Si(111) are discussed in sections 5 and 6. Finally, we discuss two important issues that give further support to the dynamical fluctuations model: the role of the defects in the transition (section 7) and many-body effects in the electronic structure (section 8). We finish in section 9 with a summary of the main conclusions.

2. The $\sqrt{3} \times \sqrt{3} \leftrightarrow 3 \times 3$ reversible phase transition

A number of different experimental techniques have been applied to characterize, both structurally and electronically, the two structures ($\sqrt{3} \times \sqrt{3}$ and 3×3) and the phase transition. The most remarkable fact is probably the apparent contradiction between the electronic and structural evidence coming from core-level spectroscopy, angle-resolved photoemission, and photoelectron diffraction (PED), supporting the presence of two inequivalent types of adatom in both the LT and the RT phases, and the findings from LEED, STM, and surface x-ray diffraction (SXRD) for the RT phase suggesting that all the adatoms are equivalent. In this section, we present the basic experimental evidence for all these systems, with special emphasis on Sn/Ge(111) and Sn/Si(111). The reason behind this puzzling contradiction between experimental techniques is presented in section 6, where the nature of the RT $\sqrt{3} \times \sqrt{3}$ phase is discussed.

2.1. The structure of the $\sqrt{3} \times \sqrt{3}$ and 3×3 phases

LEED and STM images acquired at RT on 1/3 ML α-Pb/Ge(111) [13] and Sn/Ge(111) [14] display features characteristic of a $\sqrt{3} \times \sqrt{3}$ symmetry. The LEED data include sharp diffraction spots characteristic of the $\sqrt{3} \times \sqrt{3}$R30° symmetry. Both filled- and empty-state STM images, acquired in the same scan but at different bias voltages, show a hexagonal array of identical protrusions (see figure 2 for Sn/Ge(111)), that previous experiments [26] and computer simulations [27] identify as Pb and Sn adatoms.

As the temperature is lowered, significant changes are observed. The low-temperature LEED pattern shows the presence of new spots characteristic of a 3×3 symmetry. This transition in structure is gradual and reversible, with an onset at $-20\,^{\circ}$C (253 K). In the case of STM, Pb adatoms no longer appear equivalent and the same 3×3 symmetry can be observed. One out of the three Pb adatoms appears brighter in the filled-state image, forming a hexagonal lattice, while the bright protrusions in the empty-state image are located at the other two Pb-adatom positions, forming a honeycomb pattern. As the sample temperature increases,

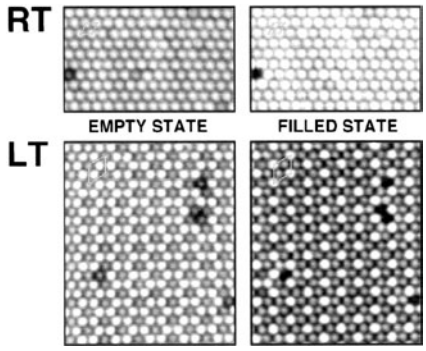

Figure 2. LT (60 K) and RT STM images for the α-Sn/Ge(111). Both occupied ($V_{sample} = +1.0$ V) and unoccupied states ($V_{sample} = -1.0$ V) are shown (after [14]).

these new 3×3 superstructures disappear and the sample returns to the equivalent adatom configuration of RT. Similar results have been obtained in the case of Sn/Ge(111), with the transition taking place at $\sim -60\,^{\circ}$C [14].

Although these measurements are indicative of the symmetry of the 3×3 phase, a complete characterization of the atomic displacements involved requires the use of more sophisticated structural techniques such as surface SXRD or PED. Apart from the first surface x-ray measurements by Baddorf *et al* [28] (who suggested a lateral distortion of the first-layer Ge atoms, with no vertical rippling), all the subsequent experimental results for Pb/Ge(111) and Sn/Ge(111) (including a combined LEED–SXRD measurement for Sn/Ge(111) [29], SXRD for Pb/Ge(111) [30], SXRD for Sn/Ge(111) [31], and PED for Sn/Ge(111) [32, 33]) clearly show that the main feature of the 3×3 phase is a vertical distortion, in which one of the adatoms is displaced outwards by around 0.3–0.4 Å relative to the other two, keeping all of them in T_4 positions, in agreement with the theoretical prediction [18] (see section 3).

As regards the structure of the $\sqrt{3} \times \sqrt{3}$ phase, SXRD measurements [29, 31]—favouring a structure with equivalent Sn adatoms—contradict PED experiments [34], where clear evidence for two inequivalent types of Sn adatom was found for temperatures up to 500 K. The detailed comparison of experiment and theoretical calculations for the 3×3 phase and a discussion of the implications of these contradictory results is left to sections 3 and 6.

At variance with the Pb/ and Sn/Ge(111) cases, the Sn/Si(111) surface shows a $\sqrt{3} \times \sqrt{3}$ symmetry in the LEED pattern and the STM images for temperatures as low as 38 K [15, 35], even in the presence of a significant density of Si substitutional defects [36]. Notice that, due to the different preparation procedures, the density of defects in Sn/Ge(111) varies between 2 and 5%, while in Pb/Ge(111) and Sn/Si(111) that density can be varied over a very wide range [37]. However, recent x-ray standing-wave experiments [38] indicate the presence of two types of Sn atom with a height difference around 0.3 Å.

Evidence on Pb/Si(111) is scarce. RHEED experiments [39] show that streaks with a 3×3 periodicity began to appear just below RT. These streaks, very weak just below RT, became slightly brighter as the temperature is lowered, but they are never as strong as the 3×3 spots observed in the Ge(111) case. However, a clear confirmation of the presence of a 3×3 transition with large domains at $T \sim 60$ K has been recently obtained with STM [15].

2.2. Electronic states in the $\sqrt{3} \times \sqrt{3}$ and 3×3 phases

2.2.1. Core levels. The 3×3 Sn 4d line shape in Sn/Ge(111) presents two components, that can naturally be associated with the two types of inequivalent Sn adatom revealed by SXRD

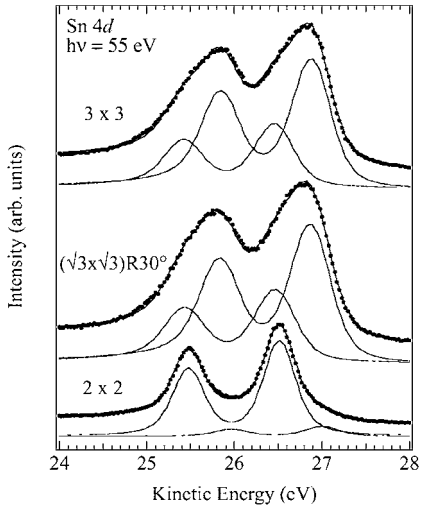

Figure 3. The Sn 4d core level for different surface reconstructions. From bottom to top, the core levels found for the 2×2, $\alpha\sqrt{3}$, and 3×3 reconstructions (after [18]).

and PED. Surprisingly, these two components are preserved, with just a small change in their relative intensities, in the $\sqrt{3} \times \sqrt{3}$ phase [18, 40, 41].

This deconvolution of the Sn 4d line shape is unique and characteristic of the $\sqrt{3} \times \sqrt{3}$ and 3×3 phases [18, 41] (see figure 3): the core level for the well-ordered 2×2 structure found for 0.25 ML coverage in Sn/Ge(111) can be fitted with a single component. The line shape for the $\sqrt{3} \times \sqrt{3}$ is much wider and can only be reproduced with two components. The intensity ratio between them is 1:2 and is not sensitive to the polar emission angle, indicating that both come from the adatom top layer. A possible relation with defects can also be discarded, since the line shape was the same for many different preparations.

These findings were challenged by Kidd *et al* [42], who obtained quite different line shapes for the RT and LT phases. While two components were enough to describe their LT spectra, the RT spectra could only be reproduced with three components. However, a combination of LEED patterns, Sn 4d line shapes, and surface state emission as a function of coverage [43] has shown that the spectra in [42] actually correspond to a line shape between the 0.20 and 0.22 ML core-level spectra, where clear 2×2 spots can be seen in the LEED pattern, and thus cannot be considered to be representative of the pure $\sqrt{3} \times \sqrt{3}/3 \times 3$ surfaces [43, 44]. The fitting of the 3×3 spectrum obtained at 70 K in [43], which is a bit more clearly resolved than previous results in the literature, requires two major components, with the approximate ratio 1:1.5, and a third small component. The two major components can be associated with the two inequivalent types of Sn adatom in the 3×3 phase, while the third small component can be associated with Sn atoms surrounding Ge substitutional defects. The intensity of this component is 10% of the total intensity, which translates into a Ge defect density of $<2\%$, in good agreement with experimental observations (typically 2–5%).

A similar deconvolution can be found for the Sn 4d line shape in Sn/Si(111) at 70 K [35]: two major components with an intensity ratio of 2:1, and a small component associated with Sn adatoms around Si substitutionals. In contrast to the case for the Sn/Ge(111) surface, the smaller Sn 4d component appears in Sn/Si(111) on the smaller-binding-energy side. At RT the Sn 4d core-level spectra look very similar except for a general broadening and they decompose into the same three components.

2.2.2. Valence band ARPES. Goldoni and Modesti [17] were the first to compare the angle-resolved photoemission spectra for the RT $\sqrt{3} \times \sqrt{3}$ and LT 3×3 phases in Pb/Ge(111) [45] and Sn/Ge(111). They found significant differences between the RT and LT spectra, with the presence of flat non-dispersive bands for the 3×3 phase, that were interpreted as evidence of the role of correlation effects in the system.

Subsequent experiments on Pb/Ge(111) [46] and Sn/Ge(111) [18, 41, 43] contradict these results. ARPES foe both systems actually shows that the $\sqrt{3} \times \sqrt{3}$ and 3×3 surfaces have almost identical band structures (see figure 4). In the Sn 3×3 case, the shape of the wide surface peak—associated with the Sn p_z states—indicates that it can be clearly decomposed into two dispersive bands, with minima at $\bar{\mathrm{K}}_{\sqrt{3}}$ (the $\bar{\mathrm{K}}$ point of the $\sqrt{3} \times \sqrt{3}$ SBZ), that corresponds to $\bar{\Gamma}_{3\times3}$ (the Γ point in the 3×3 SBZ; see 5). One of these bands crosses the Fermi level around $\frac{1}{2}\bar{\Gamma}\bar{\mathrm{K}}_{\sqrt{3}}$ ($\bar{\mathrm{M}}_{3\times3}$). The $\sqrt{3} \times \sqrt{3}$ RT spectra might, at first glance, be interpreted as one downward-dispersing peak. However, a closer look reveals a significant asymmetry of the peak for all emission angles, which is not consistent with a one-peak interpretation. The fitting procedure actually reveals two surface states, in close resemblance to the 3×3 case. These two components become more intense and narrower as we lower the temperature, which makes their detection easier. The dispersions of the two bands, obtained from the fitting procedure, are very similar for the two phases (see figure 4).

The electronic structure is very similar in the Sn/Si(111) case [35]. The appearance of the ARPES spectra is more or less the same throughout the temperature interval (RT to 70 K), and from the asymmetric peak shape across the angle series one can conclude the presence of two surface state structures, despite the fact that no 3×3 periodicity could be detected by means of structural techniques such as LEED or STM. The surface band structure is metallic, with a fully occupied band and another one crossing E_F. These two surface bands close to E_F are not as clearly resolved at low T as they are in the Sn/Ge(111) case.

Angle-resolved inverse photoemission has been applied to study the unoccupied electronic structure of Sn/Si(111) [37, 47]. In addition to a partly occupied surface band crossing E_F, there is a second surface state located 1.5 eV above E_F. The existence of these two surface states is not compatible with a $\sqrt{3} \times \sqrt{3}$ structure and can be explained, once many-body effects are introduced, in terms of two types of Sn adatom originating from an underlying 3×3 structure, as discussed in section 8.

2.2.3. Metal–insulator transition and Fermi surface nesting. The first experiments by Carpinelli *et al* [13] suggested that the transition to the 3×3 phase in Pb/Ge(111) was accompanied by a metal–insulator transition. The evidence came from the differences between the LT and RT electron energy-loss spectroscopy (EELS) spectra. The RT EELS spectrum shows a continuum of energy losses that is naturally associated with a metallic system. The presence of a discrete loss onset in the LT spectra was interpreted as an indication of the opening of a small band gap ($E_g \leqslant 0.065$ eV at 100 K) [13]. However, a subsequent EELS study by Petaccia *et al* [48] shows that the important role of image resonances in the EELS spectra of this system makes its interpretation very difficult and, thus, challenges the direct association of the discrete loss onset in the LT spectra with a metal–insulator transition. A similar study on the Sn/Ge(111) [14] shows no difference between the RT and LT EELS spectra, indicating that the system remains metallic across the transition.

ARPES provides an alternative way to characterize the Fermi surface of the system and to determine its metallic character. The ARPES spectra of Pb/Ge(111) [46] and Sn/Ge(111) [18, 41] (see figure 4) clearly show for both phases the existence of dispersive bands crossing E_F in both $\bar{\Gamma}\bar{\mathrm{K}}_{\sqrt{3}}$ and $\bar{\Gamma}\bar{\mathrm{M}}_{\sqrt{3}}$ directions, indicating that both phases are metallic.

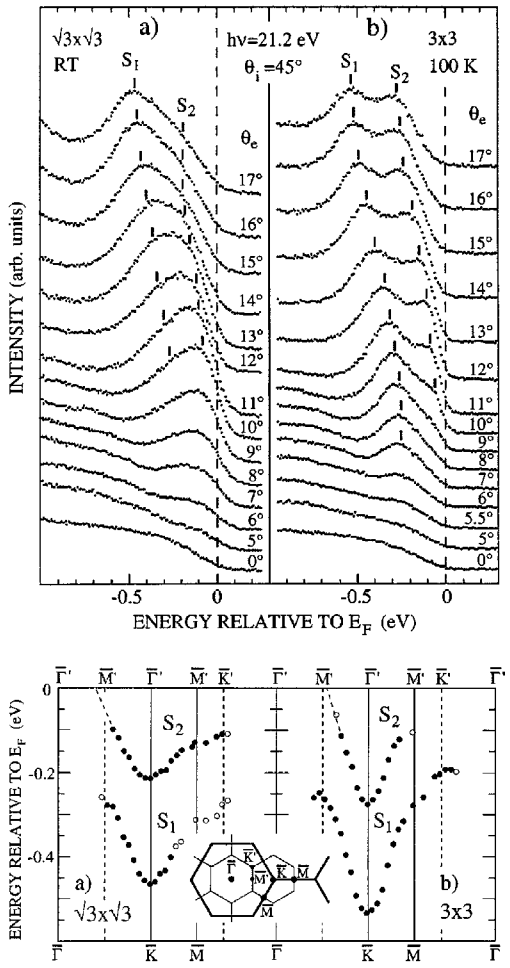

Figure 4. Top: angle-resolved valence band spectra obtained for the $\sqrt{3} \times \sqrt{3}$ (a) and the 3×3 (b) surfaces along the $\bar{\Gamma}\bar{K}_{\sqrt{3}}$ line. Two dispersive surface state bands, S_1 and S_2, are indicated by tick marks. Bottom: experimental surface band dispersions along the major symmetry lines of the $\sqrt{3} \times \sqrt{3}$ SBZ. Symmetry points for $\sqrt{3} \times \sqrt{3}$ and 3×3 are shown in the inset. Open circles indicate an uncertainty in the energy position (after [41]).

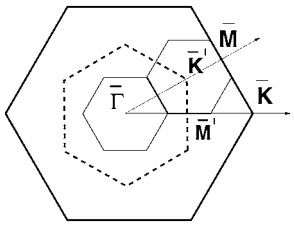

Figure 5. The surface BZ for the 1×1 (thick line), $\sqrt{3} \times \sqrt{3}$ (dashed line), and 3×3 (thin line) reconstructions. The arrows indicate the $\bar{\Gamma}\bar{K}$ and $\bar{\Gamma}\bar{M}$ symmetry directions for the 1×1 structure. Symmetry points for $\sqrt{3} \times \sqrt{3}$ ($\bar{K}'$ and $\bar{M}'$) are also indicated.

The Fermi surface presents a general undulating character [46, 49], but care has been taken in determining the presence of nesting around some symmetry points at the 3×3 BZ boundary (theoretical calculations suggest the existence of nesting in α-Pb/Ge(111) [13] but not in Sn/Ge(111) [14]). Two different procedures (parabolic fitting and the study of the modulation of the intensity at E_F) [46, 49] yield a crossing close to the mid-point in the $\bar{\Gamma}\bar{K}_{\sqrt{3}}$ direction ($\bar{M}$ point in the 3×3 SBZ) corresponding to a Fermi momentum of 0.30 ± 0.02 or 0.34 ± 0.03 Å^{-1} for the two procedures. The presence of nesting only at this single point in the direction $\bar{\Gamma}\bar{K}_{\sqrt{3}}$, that represents a very small percentage of the electronic states at E_F, is not enough to stabilize a SCDW. Other experiments on Sn/Ge(111) [49, 50] show that the Fermi surface shapes are similar in Pb and Sn/Ge(111), although no nesting appears in this case.

Sn/Si(111) is not so well characterized, but ARPES measurements for Sn/Si(111) clearly show a dispersive band crossing E_F in the $\bar{\Gamma}\bar{K}_{\sqrt{3}}$ direction [35], indicating the metallic character of the system. This is confirmed by angle-resolved inverse photoemission experiments [37, 47], where a partly occupied surface band crossing E_F is observed.

2.3. Characterizing the transition: order and temperature

Most of the experimental efforts to characterize the nature of the $\sqrt{3} \times \sqrt{3} \leftrightarrow 3 \times 3$ transition have been devoted to the determination of the local structure of the two phases. However, the temperature behaviour of the diffraction pattern, the surface order parameter that describes the thermodynamics of the whole system, provides a direct way to characterize the transition. However, problems arise due to the presence of finite-size domains and defects, as discussed below. Floreano *et al* [51] have measured the surface order parameter in Sn/Ge(111) using He-atom scattering (HAS). This technique is only sensitive to the surface charge density (like STM), is a long-range-order probe, and offers the advantage of a short interaction time (10^{-13} s).

Floreano *et al* have monitored, for few temperatures throughout the transition, the different evolutions of the diffraction peaks along the [112] direction, that are characteristic of the 3×3 phase, and the $[1\bar{1}0]$ direction, which relate also to the $\sqrt{3} \times \sqrt{3}$ phase. While the $[1\bar{1}0]$ peaks show a Debye–Waller attenuation and no variation in the width, the steeper decrease of the peak intensity and the strong broadening of the fractional-order peaks in the [112] direction indicates a strong decay of the 3×3 long-range order, thus suggesting the occurrence of an order–disorder phase transition [51]. Notice that the average size of the 3×3 domains (that can be estimated from the peak width well below T_c) has a definite influence on the T_c observed: $T_c \sim 180$ K (220 K) is observed for a mean 3×3 domain size of 200 (400 Å) [51].

The experimental determination of the critical exponents from the evolution with temperature of both the peak intensity and the Lorentzian width (proportional to the inverse of the correlation length) of the $(-2/3, 0)$ diffraction peak confirms that the system belongs to the three-state Potts universality class [51] (recall the threefold symmetry of the triangular surface lattice). The Lorentzian width displays a slight broadening below 220 K, possibly due to residual defects, while a much stronger broadening sets in above 220 K, when the order parameter intensity is also strongly reduced. The Lorentzian width can be fitted with the predicted $\nu = 5/6$ critical exponent, giving a transition temperature of 217 K. However, this transition temperature does not yield a satisfactory power law fit to the peak intensity; the expected $\beta = 1/9$ critical exponent is obtained for a slightly higher transition temperature of 223 K.

These discrepancies are related to the rounding of both the order parameter and its correlation length close to T_c due to the presence of defects within the 3×3 domains [51]. This has been illustrated in the order–disorder c$(4 \times 2) \leftrightarrow (2 \times 1)$ transition on the (001) surfaces of both Ge and Si. Due to defects, the expected two-dimensional Ising critical exponents

have only recently been found for Ge [52], and are still lacking for Si(001). This surface is strongly affected by point defects, that reduce the order parameter below T_c and smear out the transition [53, 54].

The different distribution of Ge impurities in Sn/Ge(111) when the temperature is varied (they were seen to lie on two 3×3 sublattices at 120 K, as opposed to the random distribution observed at 165 K) led the authors of [22–24] to conclude that the transition is driven by a defect–defect interaction mediated by a SCDW. They show that the STM images can be described by a superposition of exponentially damped waves with 3×3 symmetry emerging from each defect. The damping is characterized by a decay length $l(T)$ than can be determined for different temperatures by looking for the best fit of the experimental STM images. When $l(T)$ becomes comparable to the average defect–defect spacing, Ge defects start to interact and realign onto a honeycomb lattice. This realignment would lock in the 3×3 phase. With the Ge defect present in their surface, the transition temperature is 105 K $\leqslant T_c \leqslant$ 120 K. Defects have also been proposed to determine a metal–semiconductor transition observed in ARPES [55]. As discussed in section 7, theoretical calculations [21] show however that the defect–defect interaction is very localized, ruling out its proposed role in driving the transition.

Although a 3×3 transition has not been observed in Sn/Si(111) for T down to 38 K, this transition, with large domains, has been recently observed at $T \sim 60$ K in Pb/Si(111) [15]. The role of defects in this transition has been explored with an analysis of the STM images in terms of exponentially damped charge waves, similar to the one performed by Melechko *et al* [22, 24]. This analysis shows that the decay lengths are much smaller in the Pb/Si(111) case, supporting the view that defect–defect interaction is not the driving force of the transition.

3. The Sn/Ge(111)-3 $\times$ 3 atomic geometry

A key element for understanding the $(3 \times 3) \leftrightarrow (\sqrt{3} \times \sqrt{3})$ transition in α-Sn/Ge(111) is the determination of the atomic geometry of the (3×3) phase, which is the ground state of the system. This goal was first achieved theoretically [18], using a combination of local orbital (FIREBALL96 [56]) and plane-wave (CASTEP [57]) density functional theory (DFT) methods: in the search for the minimum-energy atomic structure, a fast and detailed exploration of the configurational phase space was first performed using the FIREBALL96 code, while the plane-wave method was subsequently used to refine the results [19]. The main feature of the Sn/Ge(111)-(3×3) reconstruction obtained in this way is a vertical distortion of the Sn layer in which one Sn atom (Sn_1; see figure 6) is displaced upwards and the other two Sn atoms (Sn_2 and Sn_3) are displaced downwards, with $\Delta z = z(Sn_1) - z(Sn_{2,3}) \sim 0.26$ Å. In other words, out of the three 3×3 sublattices that form the $\sqrt{3} \times \sqrt{3}$ lattice, 'up' Sn adatoms (Sn_u) occupy one of these sublattices (say 'a'), forming a 3×3 *hexagonal* lattice, while sublattices 'b, c' are occupied by 'down' Sn adatoms (Sn_d) (forming a *honeycomb* pattern). As shown in table 1, the distortion in the Sn layer is accompanied by a related distortion in the first four Ge layers. The upward and downward movements of the Sn adatoms are interconnected (see figure 6 and table 2): as one of the Sn atoms (Sn_1) moves upwards, the three Ge nearest neighbours (A_1) follow this motion by moving towards it (with both upward and in-plane displacements). These Ge displacements force corresponding in-plane movements of the Ge (labelled D_2) towards the position of Sn_1. Since the Ge D_2 atoms are also bonded to first-layer Ge atoms (B_1, C_1) linked with the two other Sn atoms (Sn_2 and Sn_3), these are forced to move downwards.

The 3×3 reconstruction shown in table 1 was found to be lower in energy than the $(\sqrt{3} \times \sqrt{3})$ surface, although only by ~5 meV per Sn atom. Similar results have been obtained in other calculations [20, 58].

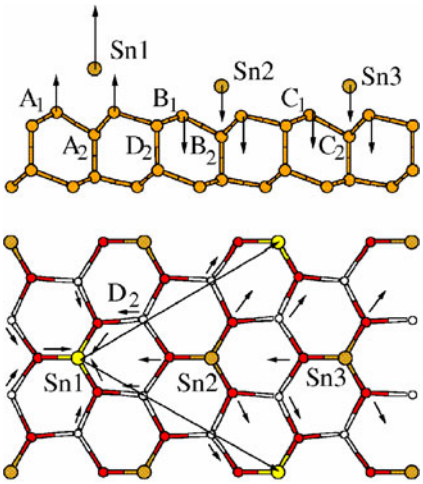

Figure 6. A ball-and-stick model of the Sn/Ge(111)-(3 × 3) reconstruction. The arrows show the direction of the atomic displacements (up/downwards at the top, in the plane in the bottom figure) w.r.t. the $\sqrt{3} \times \sqrt{3}$ geometry. Notice that the Ge atoms move in the plane towards the position of the upper (Sn_1) and away from the two other Sn atoms. The atoms D_2 connect the Ge atoms which are nearest neighbours of the different Sn atoms.

Table 1. Main structural parameters (in Å) for the Sn/Ge(111)-(3 × 3) reconstruction. Δz_i is the vertical displacement of the different atoms in each layer with respect to the average layer vertical position, and $\Delta\perp_1$ corresponds to the inwards in-plane displacements of the first-layer Ge atoms, referred to the ideal (111) surface (in table 2 these displacements are measured with respect to the *flat* $\sqrt{3} \times \sqrt{3}$ surface). The theoretical atomic structure [19] is compared with two experimental data sets, from LEED/SXRD [29] and SXRD [31]; see [19] for more details.

		Theory	LEED/SXRD	SXRD
Δz_0	A_0	+0.18	+0.25	+0.17
	B_0	−0.08	−0.12	−0.07
	C_0	−0.08	−0.12	−0.10
Δz_1	A_1	+0.10	+0.11	+0.07
	B_1	−0.05	−0.06	−0.04
	C_1	−0.06	−0.06	−0.04
Δz_2	A_2	−0.36	−0.37	−0.42
	B_2	−0.39	−0.37	−0.35
	C_2	−0.39	−0.37	−0.43
	D_2	+0.18	+0.19	+0.20
$\Delta\perp_1$	A_1	0.20	0.17	0.19
	B_1	0.12	0.05	0.17
	C_1	0.12	0.05	0.18

The vertical rippling found in the theoretical calculation has been confirmed by all the structural experiments performed so far for the 3 × 3 phase of Sn/Ge(111), including a combined LEED–SXRD measurement for Sn/Ge(111) [29] (Sn height difference of 0.37 Å), SXRD (0.26 Å) [31], and PED studies (0.31 Å) [32, 33]. The theoretical 3 × 3 atomic geometry is compared in detail in table 1 with the results of these structural studies. The overall agreement between the theoretical displacements and the experimental data is remarkable, giving strong support to the proposal that in the Sn/Ge(111)-3 × 3 surface the Sn layer is distorted, with one

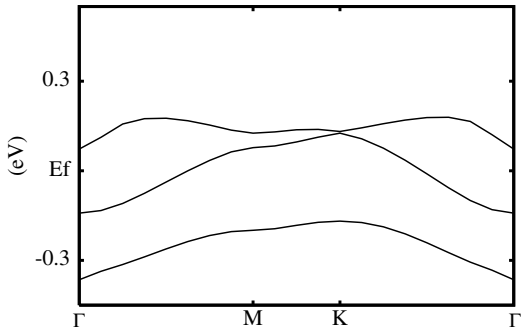

Figure 7. Electronic structure of the Sn/Ge(111)-(3 × 3) surface: surface band structure, along the symmetry directions in the 3 × 3 SBZ, obtained from LDA calculations with three bands corresponding to the dangling bonds of the Sn_1 (lower band) and the Sn_2, Sn_3 atoms from figure 6.

Table 2. Atomic displacements (in Å) associated with the Sn/Ge(111)-(3 × 3) surface measured w.r.t. the $\sqrt{3} \times \sqrt{3}$ geometry [20].

	Sn_1	Sn_2	Sn_3	A_1	B_1	C_1	A_2	B_2	C_2	D_2
Δz	0.18	−0.08	−0.08	0.08	−0.04	−0.03	0.02	0.00	0.00	0.00
$\Delta\perp$	0.00	0.00	0.00	−0.04	0.02	0.02	0.00	0.00	0.00	0.04

Sn adatom up and two Sn adatoms down, with $\Delta z \sim 0.3$ Å. A similar 3 × 3 reconstruction has also been found for the Pb/Ge(111) system [30], with a height difference between inequivalent Pb atoms of 0.4 Å.

4. The Sn/Ge(111)-3 × 3 electronic structure (1): occupied states

Extra support for the atomic structure shown in figure 6 and table 1 comes from the analysis of its electronic structure. Figure 7 shows the Sn/Ge(111)-(3 × 3) LDA surface bands appearing close to E_F, as calculated with FIREBALL96. These three bands are associated with the three Sn dangling bonds. Each of these dangling-bond states is basically spread over six atoms, say Sn_1, the Ge atoms A_2, A_3, and the three A_1s, for the dangling bond associated with the lower band. For the Sn atom displaced upwards (Sn_1), rehybridization makes its dangling bond have a more s-like character and a corresponding lower energy. The lower surface band in figure 7 is associated with that atom and it is doubly occupied. On the other hand, the other two surface bands, located around E_F, are associated with the two dangling bonds of the Sn atoms displaced downwards (Sn_2, Sn_3). Thus, these dangling bonds share the remaining electron and are, on average, only occupied by half an electron. Notice that in the change from an *ideal* (or *flat*) $\sqrt{3} \times \sqrt{3}$ surface to the 3 × 3 reconstruction the number of partially filled dangling bonds is further reduced, from 3 to 2 /3 × 3 unit cell.

The occupied DOS close to E_F was measured using valence band PES [18, 41]. These experiments show that the Sn/Ge(111)-(3 × 3) surface presents two dispersive surface states below E_F, one of them crossing E_F (see figure 4). The widths of these two states are ∼0.2–0.3 eV, both reaching their minimum value at the $\bar{\Gamma}$ point of the (3 × 3) BZ. The lower band is ∼0.2–0.3 eV below the upper one. All these features are in good agreement with the theoretical result (see figure 7), therefore further supporting the structural model for this surface discussed above.

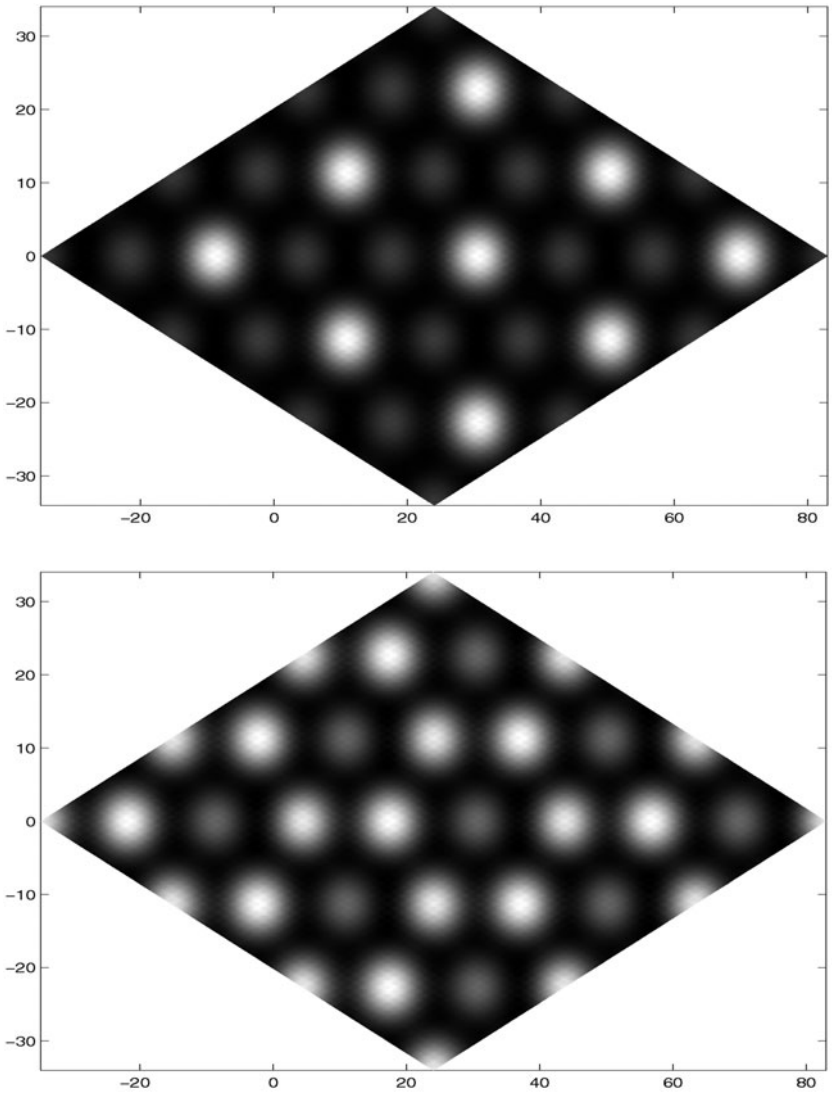

Figure 8. Calculated STM images of the occupied (top, $V_{bias} = -0.55$ V, tip–sample distance 5.12 Å) and unoccupied (bottom, $V_{bias} = +0.55$ V, tip–sample distance 4.25 Å) states at the Sn/Ge(111)-(3 × 3) surface simulated in constant-height mode (after [59]). Coordinates are given in au.

The (3 × 3) surface reconstruction shown in table 1 also explains the LT STM images. Figures 8(a) and (b) show the calculated STM images, for occupied and unoccupied states, obtained for the Sn/Ge(111)-(3 × 3) geometry and electronic structure discussed above [59]. The STM image for the occupied states shows the 'up' Sn adatoms (Sn_1 or Sn_u) as bright protrusions: in this case the tunnelling takes place from occupied states which are mainly localized in Sn_u adatoms. On the other hand, in the positive-bias image the 'down' adatoms ($Sn_{2,3}$ or Sn_d) appear brighter than the 'higher' Sn_u adatoms since the empty states are localized in the Sn_d adatoms (see [59] for details).

5. Two questions

The discussion of the preceding sections shows that we have a good knowledge of the α-Sn/Ge(111)-3×3 ground state atomic structure. Once we understand the atomic geometry of the LT phase, two questions emerge:

(1) What is the atomic structure of the Sn/Ge(111)-$\sqrt{3} \times \sqrt{3}$ high-temperature phase?
(2) What is the driving force for the $\sqrt{3} \times \sqrt{3} \leftrightarrow 3 \times 3$ phase transition?

These questions are interconnected, and are the subject of the following section. The clue that will help us answer them is the experimental similarities of and differences between the α-Sn/Si(111) and α-Sn/Ge(111) surfaces. As mentioned in section 2, these two systems present very similar behaviours at RT, but the Sn/Si(111) system does not present the transition to the 3×3 phase for temperatures down to 38 K.

6. A surface soft phonon

Experiments show that the electronic structure of the α-Sn/Si(111) surface is very similar to the Sn/Ge(111) one. Photoemission data display two major components in the Sn 4d core-level spectra and two surface bands close to the Fermi level [35], although these two surface bands are not as clearly resolved at low T as they are in the Sn/Ge(111) case. Thus, it seems natural to wonder whether the α-Sn/Si(111) surface also presents a similar 3×3 reconstruction at LT. This possibility has been explored by means of DFT calculations [20]. In this analysis, we start from a $\sqrt{3} \times \sqrt{3}$ structure (in a 3×3 unit cell), where the three Sn atoms are equivalent; we select one of them (Sn_1) and force it to move in the direction perpendicular to the surface. For each of these displacements, the other Sn atoms (Sn_2 and Sn_3) and all the semiconductor atoms are allowed to relax (up to the fifth layer) to their zero-force positions under the constraint of the Sn_1 displacement. These calculations were performed for both the α-Sn/Si(111) and α-Sn/Ge(111) surfaces (see figure 9(a)). The energy versus Sn_1 displacement is very flat for Sn/Ge(111); the ground state corresponds to the 3×3 reconstruction discussed above, with a Sn_1 displacement of $\sim$0.18 Å. The Sn/Si(111) surface, however, does not present any stable 3×3 distortion, i.e., the *flat* $\sqrt{3} \times \sqrt{3}$ structure is the stable structure at low T.

In figure 9(b) we see that in both systems the adatoms Sn_2 and Sn_3 move together in the opposite direction to the constrained motion of the Sn_1 atom. This result suggests a correlated up/down motion of the Sn atoms that, at a sufficiently LT, is frozen into the 3×3 structure in the case of α-Sn/Ge(111), but not in the case of α-Sn/Si(111). The normal modes associated with this correlated up/down motion have been analysed introducing a force constant model based on the DFT calculations reflected in figure 9 [20]. Figures 10(a) and (b) show the phonon dispersion curves for α-Sn/Ge(111) and α-Sn/Si(111), compared with the projected phonon bulk band structures of Ge and Si. Notice that, for α-Sn/Ge(111), *a zero-frequency mode* is found at the $\bar{K}'$ ($K_{\sqrt{3}}$) point which, in fact, corresponds to *a reciprocal-lattice vector of the 3 × 3 periodicity*. This *surface soft phonon* is intimately related to the $\sqrt{3} \times \sqrt{3} \leftrightarrow 3 \times 3$ reversible phase transition in α-Sn/Ge(111) [20]: at low T the $\sqrt{3} \times \sqrt{3}$ surface becomes unstable with respect to the atomic displacements of the soft mode, and undergoes a transition to the lower-symmetry 3×3 phase. For α-Sn/Si(111), the phonon dispersion relation shows only a minimum at the $\bar{K}'$ point, with a phonon energy of 5.5 meV: as shown in figure 9(a), the flat $\sqrt{3} \times \sqrt{3}$ structure is the stable structure at low T in this case. Notice that, in the case of α-Sn/Ge(111), anharmonic effects should renormalize, at RT, the frequency of the soft mode to a non-zero value, as indicated schematically in figure 10(a).

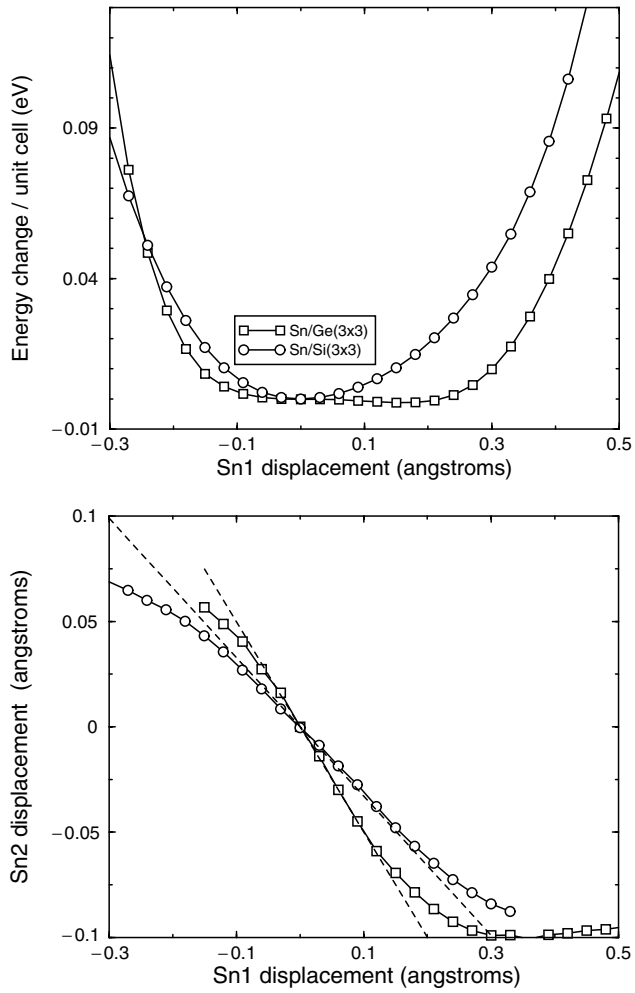

Figure 9. Top: total energy as a function of the Sn_1 displacement (see figure 6) for the Sn/Ge(111) (squares) and Sn/Si(111) (circles) surfaces. The energy of the $\sqrt{3} \times \sqrt{3}$ structure is taken as the reference. Bottom: displacements (in Å) of the Sn_2, Sn_3 atoms as a function of the Sn_1 displacement. All the displacements are referred to the $\sqrt{3} \times \sqrt{3}$ structure (after [20]).

These results help us to understand the origin of the main similarities and differences observed for the α-Sn/Ge(111) and α-Sn/Si(111) surfaces. At low T, while for the α-Sn/Ge(111) surface we can expect a phase transition to the 3×3 structure, there is no stable 3×3 phase for the α-Sn/Si(111) surface. On the other hand, the vibration associated with the 3×3 structure is a minimum of the phonon dispersion for both systems. Thus, at a high enough temperature (say, for $k_B T \gg 6$ meV, room temperature is a high-T limit) the two surfaces can be expected to behave in similar manners. This can be understood by considering the energy curves in figure 9(a): at room temperature the Sn atoms vibrate with a large amplitude in both surfaces (with displacements between -0.2 and 0.3 Å for Sn/Ge(111) and -0.2 and 0.2 Å for Sn/Si(111)). In this vibration, Sn atoms are correlated with their Sn nearest neighbours, as shown in figure 9(b).

We are now ready to discuss the dynamical effects that give rise to the $\sqrt{3} \times \sqrt{3}$ symmetry observed for the α-Sn/Ge(111) high-temperature phase. At room temperature, the surface soft

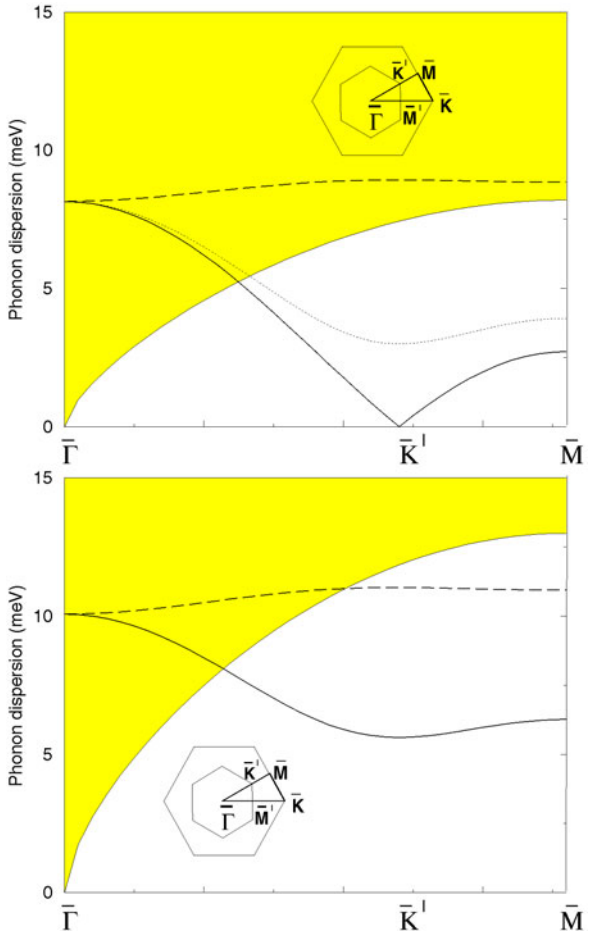

Figure 10. Phonon dispersion curves for the Sn/Ge(111) (full curve, top) and Sn/Si(111)-$\sqrt{3} \times \sqrt{3}$ (full curve, bottom) surfaces. Dashed curves correspond to the H-saturated Sn/Ge(Si)(111)-$\sqrt{3} \times \sqrt{3}$ surfaces. Shaded areas represent the projection of the corresponding phonon bulk band structure. The phonon branches are plotted along the $\bar{\Gamma}\bar{M}$ direction in the first Brillouin zone (BZ) of the ideal (111) surface (see the inset). The inner hexagon corresponds to the BZ of the $\sqrt{3} \times \sqrt{3}$ surface. $\bar{K}'$ defines the new 3×3 periodicity associated with the soft phonon in Ge. At room temperature, the frequency of the soft mode should be renormalized to a non-zero value, as shown schematically by the dotted curve (after [20]).

phonon is only one of the many vibrational modes that contribute to the atomic motion of the α-Sn/Ge(111) surface. A deeper insight into this atomic motion may be obtained from the results of first-principles molecular dynamics simulations [18]. These computer simulations show that, at LT, the Sn adatoms display large vertical displacements (0.2–0.3 Å) while keeping the (3×3) periodicity, i.e. one of the three Sn atoms per 3×3 unit cell oscillates around a higher position than the other two. When the temperature is increased (e.g. $T \sim 250$ K) the oscillations become larger and an interesting process takes place: at certain moments two Sn atoms interchange 'heights' (while staying at the same T_4 site), the upper Sn atom becoming one of the two lower Sn atoms, and one of the lower Sn atoms becoming the upper Sn atom. These *dynamical fluctuations* explain the different experimental observations for the

Sn/Ge(111)-$\sqrt{3} \times \sqrt{3}$ surface, once the timescales of the different experimental techniques are compared with the timescale of the dynamical fluctuations, t_{DF} (the FIREBALL96 simulations mentioned above give the rough estimate of $t_{DF} \sim 10^{-12}$ s). For example, STM, with a timescale of $t_{STM} \sim 10^{-3}$ s, measures the average position of the Sn atoms and, therefore, in the STM images at RT all the Sn atoms are equivalent, with a $\sqrt{3} \times \sqrt{3}$ symmetry. On the other hand, in PES experiments ($t_{PES} \sim 10^{-15}$ s) an 'instantaneous picture' of the system is obtained, typically with one Sn atom 'up' and two Sn atoms 'down'. This explains the similarity of the electronic structures of the $\sqrt{3} \times \sqrt{3}$ and 3×3 phases, as measured in PES experiments.

As mentioned in section 2, SXRD measurements for the RT phase [29, 31] find the average position of the Sn atoms to correspond to a flat $\sqrt{3} \times \sqrt{3}$ structure. These experiments also provide information about the vibrational amplitudes. The SXRD data of Bunk *et al* [31] seem to rule out the large RT vibrations predicted by the dynamical fluctuations model, but recent SXRD data [60], with access to a larger number of the crystal truncation rods [25], show that a structural model incorporating large vibrations gives the best fit to the experimental data.

However, the best evidence for the dynamical nature of the RT phase comes from PED experiments [34]. In this technique, the photon energy dependence of the intensity ratio between the two core-level components of the Sn 4d core level is measured for a range of temperatures. These experiments show conclusively that in the $\sqrt{3} \times \sqrt{3}$ structure there are two inequivalent types of Sn adatom with different bonding geometries (different vertical distances between Sn and the Ge atom underneath) up to a temperature of 500 K.

In the case of Sn/Si(111) the evidence is very scarce, but recent x-ray standing-wave experiments [38] indicate the presence of two types of Sn atom with a height difference around 0.3 Å, in good agreement with the dynamical fluctuations model.

Structural phase transitions have been traditionally classified into two different types: displacive transitions, associated with small displacements from a higher-symmetry reference structure due to the presence of a soft mode, and order–disorder transitions [61]. The He scattering data on Sn/Ge(111) have been interpreted as being in favour of an order–disorder transition [51]. However, it is known that the distinction between the two types is not necessarily clear [25], and that, over large temperature ranges, a displacive transition may give rise to order–disorder-like dynamics [61]. Recent PED experiments [34] confirmed that this order–disorder character remains up to 500 K, ruling out the presence of a transition to a flat $\sqrt{3} \times \sqrt{3}$ structure. Thus, the $\sqrt{3} \times \sqrt{3} \leftrightarrow 3 \times 3$ case supports the view prevailing nowadays that real phase transitions share features from these two extreme models: the softening of a 3×3 surface phonon provides the driving force behind the LT structure, while the RT phase—incompatible with the static $\sqrt{3} \times \sqrt{3}$ structure that one would expect from a displacive transition—can only be understood from the point of view of an order–disorder transition driven by the dynamical fluctuations of the underlying 3×3 structure.

The comparison of the α-Sn/Ge(111) and α-Sn/Si(111) cases has also been exploited to analyse the physical mechanism that leads to the 3×3 reconstruction. As Si and Ge are isovalent atoms and the electronic structures of the two interfaces are very similar, one might expect the difference in relative stability of the *flat* $\sqrt{3} \times \sqrt{3}$ and 3×3 structures to be related to the different elastic properties of the two materials. In order to separate the elastic energy contribution from the electronic energy associated with the surface band splitting induced by the 3×3 distortion [19], the Sn/Ge(111) and Sn/Si(111) surfaces with hydrogen atoms saturating the Sn dangling bonds have also been studied [20]. As shown in figures 10(a) and (b), the dispersion curves for the H-saturated surfaces do not display the 'softening' of the mode at $\bar{\mathrm{K}}'$, this result suggesting that the surface soft phonon (and therefore the 3×3 reconstruction) is due to the surface band splitting (or Sn dangling-bond rehybridization).

In order to quantify these effects, we have considered the relaxed Sn surfaces discussed above (see figure 9) for two different Sn_1 displacements, namely, 0.0 Å (the flat $\sqrt{3} \times \sqrt{3}$ geometry) and 0.18 Å (the '3×3' geometry). The elastic contribution is calculated, in each case, as the difference in energy between the two geometries *with H atoms saturating the Sn dangling bonds*. Subtracting this elastic contribution from the total-energy difference for the Sn surfaces, the energy contribution due to the Sn dangling-bond rehybridization is obtained. These calculations provide the following results: $E_{elastic}(\mathrm{Ge}) = 156$ meV and $E_{electronic}(\mathrm{Ge}) = -158$ meV; $E_{elastic}(\mathrm{Si}) = 131$ meV and $E_{electronic}(\mathrm{Si}) = -112$ meV. Therefore, the main difference between the Sn/Ge(111) and Sn/Si(111) cases is the difference in hybridization between Sn and the surface atoms. A comparison of the surface bands for the two cases confirms this result: the Ge case presents in the 3×3 geometry a larger band splitting: 152 meV as compared with 93 meV for Si. This effect can be related to the different sizes of Si and Ge [62]. When Sn is closer in size to the semiconductor atom, the surface rehybridization is stronger and the surface gains more energy by means of the surface band splitting caused by the 3×3 distortion.

In summary, the mechanism behind this phase transition is the electronic energy gain associated with the surface band splitting induced by the 3×3 reconstruction, that overcomes the elastic energy spent in the deformation of the system. The same mechanism lies behind the asymmetric structure of the dimers appearing on the (001) surfaces of both Si and Ge, where the tilting favours, via a further rehybridization of the atomic sp^3 orbitals, an additional splitting of the two bands and an associated energy gain. A phase transition is observed in these surfaces between the $c(4 \times 2)$ structure in which these asymmetric dimers order at LT and a 2×1 phase at RT due to the fluctuations of the dimer atoms between the two possible asymmetric configurations [6].

Notice that neither the experiments nor the theoretical calculations (see section 2.2.3) support the presence of nesting in Sn/Ge(111) and that our arguments prove that the existence of a surface charge-density wave (SCDW) cannot be the driving force behind the transition.

7. The role of defects in the $\sqrt{3} \times \sqrt{3} \leftrightarrow 3 \times 3$ phase transition

Point defects—with an average concentration of 2–5% [22, 36, 63]—are always present on these surfaces and their properties may affect the $\sqrt{3} \times \sqrt{3} \leftrightarrow 3 \times 3$ phase transition. 90% of those defects for Sn/Ge(111) are Ge substitutionals, while vacancies account for the other 10% [22]: we shall concentrate on discussing the properties of Ge substitutionals that we will call Ge defects in the rest of the section.

STM, a real-space experimental technique, has been the method of choice for getting non-averaged information on the structure and distribution of these defects on Sn/Ge(111) across a wide temperature range, covering the transition temperature, T_c [22, 23]. The data collected by the authors of [22, 23] show that

(a) at RT, Ge defects are imaged as dark spots in the $\sqrt{3} \times \sqrt{3}$ lattice surrounded by six features, brighter than Sn adatoms away from defects, that correspond to the six nearest-neighbour (nn) Sn adatoms;
(b) at RT, Ge defects are randomly distributed over the three 3×3 sublattices that form the $\sqrt{3} \times \sqrt{3}$ lattice;
(c) at LT most of the Ge defects occupy positions corresponding to the two honeycomb Sn_d sublattices b, c (see section 3), with equal probability, and are therefore surrounded by three bright and three darker Sn nn, at variance with the RT case for which each defect sees a sixfold symmetry around itself.

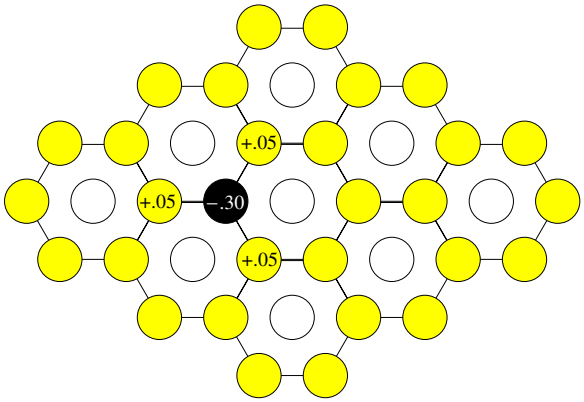

Figure 11. (a) Relaxed structure for the isolated defect. Only the vertical displacements (in Å) with respect to the ideal 3×3 structure which are larger than 0.01 Å are indicated. Notice that the distortion is confined to the defect site (black circle) and the three neighbouring Sn atoms with partially occupied dangling bonds (grey circles). Sn atoms with fully occupied DBs are indicated by white circles.

These results have been considered as supporting evidence for an interpretation of the $\sqrt{3} \times \sqrt{3} \leftrightarrow 3 \times 3$ phase transition in terms of the interaction between Ge defects [22–24]. One of the main ingredients in the argument is the difference between the symmetries that a Ge defect sees at low and high temperatures: threefold in the first case, sixfold in the second. This change of symmetry has been explained as due to a long-range interaction between defects, which would be responsible of the ordering of defects at LT on two of three possible sublattices. The superposition of the perturbations induced by defects located in these two sublattices would give rise to the 3×3 phase and threefold symmetry appearing around each defect.

We have analysed the relationship between Ge defects and the $\sqrt{3} \times \sqrt{3} \leftrightarrow 3 \times 3$ phase transition using DFT-LDA simulations [21]. In particular, we have studied the atomic geometry, the electronic structure, and the energetics of one or two defects in a large 9×9 unit cell. Our analysis supports a completely different point of view: both the structure and the ordering of the Ge defects at LT are induced by the ground state 3×3 reconstruction.

Figure 11 shows the relaxed geometry obtained in our calculations for the α-Sn/Ge(111) surface with one Ge defect /9×9 unit cell (3.7% concentration). The surface presents the 3×3 reconstruction with the Ge adatom at one of the two 3×3 sublattices (say 'b') that form the honeycomb pattern associated with Sn_d adatoms. Our simulations yield for the Ge substitutional a downwards displacement of 0.3 Å. with respect to the original Sn_d position. An important result appearing in the calculations is that the perturbation induced by the Ge defect is well localized, affecting only to the three nn. Sn_d adatoms (c sublattice) move upwards by ∼0.05 Å. The rest of the Sn atoms are located practically at the same positions as in the 3×3 reconstruction free of defects. The STM image of this isolated [21] defect presents a threefold symmetry around the Ge defect. Notice that the solution shown in figure 11 is twofold degenerate: an equivalent solution is obtained by applying a symmetry operation that exchanges the two sublattices (a, c) occupied by Sn_u and Sn_d atoms. This degeneracy will be important when discussing the effect of temperature on the surface geometry and its corresponding STM image.

In order to understand how defects interact, we have analysed the relaxed surface geometry for two Ge defects on first-, second-, and third-nn positions. Figures 12(a)–(c) show our results. In all the cases, the 3×3 reconstruction adapts its particular geometry (from a threefold-degenerate case) to the Ge defect positions in such a way that the two Ge defects are always

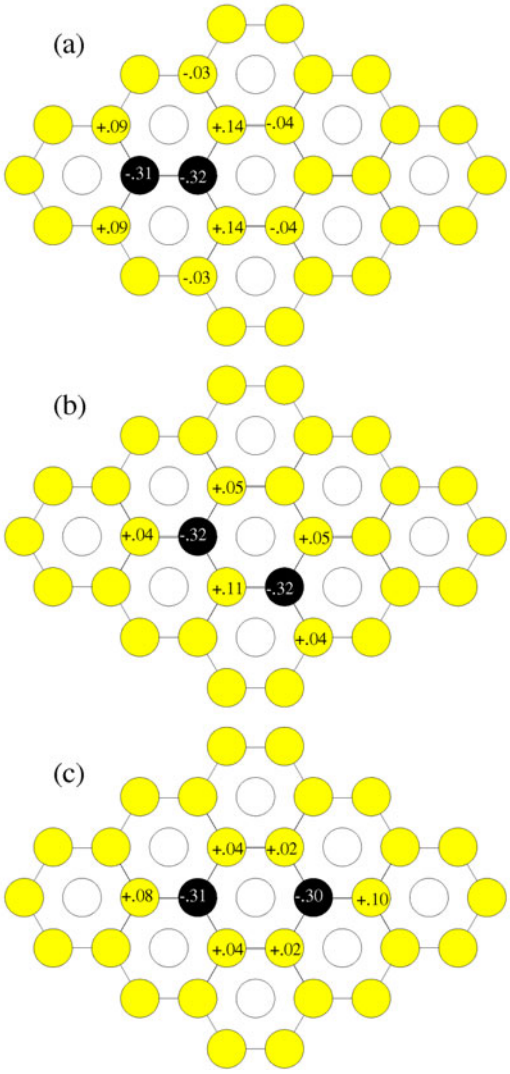

Figure 12. Relaxed structures (as in figure 11) for two Ge defects on first-nn (a), second-nn (b) and third-nn (c) positions [21].

placed on the two Sn_d sublattices forming a honeycomb pattern. As in the case of an isolated defect, the perturbation induced by the defects is localized essentially on the Sn_d atoms that are nn to the Ge defects. The total energies of the three cases are, within the accuracy of our calculations (around 20 meV /9 $\times$ 9 unit cell) the same, confirming the localized nature of the distortion induced by the Ge defects.

Coming back to the experimental STM data for the Ge defects on the Sn/Ge(111) surface, we first notice that our solution for a single defect (figure 11) has a threefold symmetry. This agrees with the images at LT, but disagrees with the experimental data at RT that show a sixfold symmetry around the defect [22]. We can resolve this apparent contradiction by considering the dynamics of the atoms around the defect. To this end, we have considered a 3 $\times$ 3 unit cell with a single Ge defect and have performed MD simulations at two different temperatures,

$T = 180$ and 270 K [21]. Our results show that Ge remains around its equilibrium site, while the two Sn atoms tend to exchange heights, very much in accord with our discussion about the dynamical fluctuations model for the $\sqrt{3} \times \sqrt{3} \leftrightarrow 3 \times 3$ phase transition. This dynamical effect explains in a simple way the different patterns observed at RT and LT on the STM images around a Ge defect and also explains why Sn adatoms that are nn to a Ge defect appear, in the RT STM images, brighter than Sn adatoms in regions free of defects.

We finally address the following question: why do Ge defects at LT occupy preferentially two 3×3 sublattices with equal probabilities, and not all three of them or only one? The results in our figure 12 provide the following explanation: a Ge substitutional defect creates a very localized perturbation on the 3×3 reconstruction, the Ge atom being located in any of the two Sn_d sublattices, replacing one of the Sn atoms that are displaced downwards. Since the defect–defect interaction is negligible, Ge defects occupy with equal probabilities any of the two sublattices of the honeycomb pattern.

From this analysis we conclude that *the ordering of Ge defects at LT is induced by the ground state 3×3 reconstruction and not the other way around*: Ge substitutional defects are not the driving force of the $\sqrt{3} \times \sqrt{3} \leftrightarrow 3 \times 3$ transition in the Sn/Ge(111) surface, although they can affect the transition temperature due to the relaxed structure shown in figure 11 that also tends to stabilize locally the 3×3 reconstruction.

8. The 3×3 electronic structure: many-body effects

We have analysed in previous sections the electronic properties of the 3×3 reconstructed surface by means of LDA calculations. In particular, figure 7 shows the LDA surface bands associated with the 3×3 ground state. Do these bands represent a fair approximation to the electronic structure of the 3×3 reconstruction? Or can we expect to have electron correlation effects that modify substantially the LDA surface bands? The importance of these effects on the surface bands depends crucially on the ratio between the effective on-site Coulomb interaction, say U_{eff}, for each dangling-bond orbital, and the surface bandwidth, W [64]. In our case, this ratio will be shown below to be larger than 1, this value indicating that electron correlation effects should be important. In this section we present a discussion of these effects and analyse how they modify the electron surface bands.

We have analysed these many-body effects [65] using the following generalized Hubbard Hamiltonian associated with the dangling bonds of the 3×3 surface:

$$\hat{H} = \sum_{\alpha,\sigma} E_\alpha \hat{n}_{\alpha\sigma} + \sum_{\alpha \neq \beta,\sigma} t_{\alpha\beta} \hat{c}^\dagger_{\alpha\sigma} \hat{c}_{\beta\sigma} + \sum_{\alpha} U_\alpha \hat{n}_{\alpha\uparrow} \hat{n}_{\alpha\downarrow} + \tfrac{1}{2} \sum_{\alpha \neq \beta,\sigma\sigma'} J_{\alpha\beta} \hat{n}_{\alpha\sigma} \hat{n}_{\beta\sigma'}, \tag{1}$$

where E_α is the energy level of the wavefunction associated with dangling bond α; $t_{\alpha\beta}$ defines the effective hopping between α and β; and U_α and $J_{\alpha\beta}$ are the on-site ($\alpha\alpha$) and off-site ($\alpha\beta$) Coulomb interactions. In equation (1), $\hat{n}_{\alpha\sigma}$, $\hat{c}^\dagger_{\alpha\sigma}$, and $\hat{c}_{\beta\sigma}$ are the occupation number, creation, and annihilation operators, respectively, and σ is the spin.

Hamiltonian (1) has been fitted to the electronic properties of our 3×3 reconstructed surface. This means that the LD solution of Hamiltonian (1) (see [66]) has been fitted to the surface band structure shown in figure 7. This fitting only yields $t_{\alpha,\beta}$ and the effective energy levels of each orbital. This is obviously not enough to determine all the parameters of Hamiltonian (1). We supplement our approach with different 'restricted LDA calculations' [67], whereby the filling factors of the different surface bands are varied and in this way the corresponding occupation numbers, $n_{\alpha\sigma}$, are changed. LDA self-consistency for the new restricted cases yields, in turn, new parameters for the effective dangling-bond levels, which are related to the new occupation numbers, $n_{\alpha\sigma}$. This procedure allows us to calculate

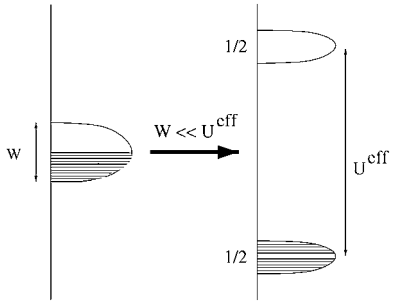

Figure 13. The metal–insulator transition for the $\sqrt{3} \times \sqrt{3}$ reconstruction: correlation effects split the half-occupied surface band into two inequivalent pieces, each one having half of the initial weight, and system becomes an insulator (after [64]).

E_α, $t_{\alpha,\beta}$, U_α, and $J_{\alpha,\beta}$ (this last parameter has been calculated, in practice, as the interaction between electrons in dangling bonds α and β). Our calculations yield the following values of U_α and $J_{\alpha,\beta}$: (a) Sn/Ge(111) surface: $U = 1.1$ eV, $J_{nn} = 0.25$ eV; (b) Sn/Si(111) surface: $U = 1.5$ eV, $J_{nn} = 0.35$ eV; where J_{nn} is the Coulomb interaction between nearest-neighbour orbitals.

Once we have determined its different parameters, we proceed to analyse the general properties of Hamiltonian (1). It is also convenient at this point to discuss the properties of an ideal (flat) $\sqrt{3}\times\sqrt{3}$ surface (with the Sn atoms having no dynamical fluctuations), and compare it with the 3×3 case. This will allow us to make some comparisons which will reinforce our general conclusions about the character of the $\sqrt{3} \times \sqrt{3} \leftrightarrow 3 \times 3$ phase transition. The $\sqrt{3} \times \sqrt{3}$ surface is characterized by having a single orbital and one electron per site and unit cell, defining a typical half-occupied band with all the sites equivalent. In this particular case, we are interested in the electron local fluctuations appearing between different spins at the same site. For this case, $U_{eff} = U - J_{nn}$ defines the on-site effective interaction between electrons of different spins. For the different cases we are considering, we find $U_{eff}(\mathrm{Sn/Si}) = 1.15$ eV and $U_{eff}(\mathrm{Sn/Ge}) = 0.85$ eV. These values are substantially larger than the corresponding bandwidths W for the $\sqrt{3} \times \sqrt{3}$ surfaces which we find to be $W(\mathrm{Sn/Ge}) = 0.38$ eV and $W(\mathrm{Sn/Si}) = 0.3$ eV. This suggests that, since in both cases $U_{eff} \gg W$, the surface bands present a Mott transition. Figure 13 shows, schematically, the physical situation: correlation effects split the surface band into two inequivalent pieces, each one having half of the initial weight.

Next, we consider the 3×3 reconstruction and the corresponding three surface bands shown in figure 7, above. We can discuss the main physics of this problem, neglecting the lowest band that is fully occupied with two electrons, and considering only the two partially filled bands associated with the two dangling bonds of the $\mathrm{Sn_d}$ atoms moving inwards. In this approximation, we find two dangling bonds and one electron per unit cell filling the surface bands. The system, as calculated in the LDA, is metallic and we are interested in its possible metal–insulator transition due to the large values of the Coulomb interactions. Figure 14 shows our system schematically, with one electron every second orbital. Can this system present a metal–insulator transition? The first point to notice is the following: a local intrasite Coulomb interaction alone cannot create in this system a Mott transition. The reason is clear: even if U is large enough to prevent two electrons from being located at the same site simultaneously, electrons can move along the crystal jumping from one site to an empty one. This shows that a metal–insulator transition can only appear in this quarter-filled band, if the intersite Coulomb

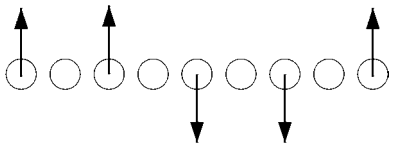

Figure 14. The metallic LDA solution for 3×3 reconstruction: we find two dangling-bond orbitals (associated with two lower Sn atoms) and a single electron per unit cell (1/4 occupancy) (after [65]).

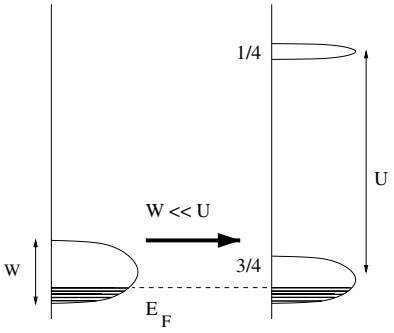

Figure 15. Correlation effects for 3×3 reconstruction: the metallic band is narrowed by 3/4 and a new peak, with 1/4 weight, is created at $E_F + U$. The system remains metallic (after [64]).

interaction is large enough to prevent electrons moving along the crystal. The effective intersite interaction, J_{eff}, is given by $\gamma J_{nn} = (Z - 1)J_{eff}$ [64], where Z is the lattice coordination number and $(1 + \gamma)J_{nn}$ defines the Madelung potential created by the charges $n_1 = 1$ and $n_2 = -1$ located on the two lattice sites. For the Sn/Ge(111)-3×3 interface, $J_{eff} = 0.20$ eV, while for the Sn/Si(111)-3×3 case we find $J_{eff} = 0.2$ eV. A metal–insulator transition associated with an intersite Coulomb interaction appears for J_{eff} larger than the bandwidth associated with the two partially filled bands. In our calculations, W is around 0.27 eV for the Sn/Si(111)-3×3 reconstruction and 0.32 eV for Sn/Ge(111)-3×3. This shows that we cannot expect to have a metal–insulator transition in those interfaces, although the Sn/Si(111)-3×3 case is not far from the transition point. Figure 15 shows schematically the kind of DOS we can expect to have in the 3×3 reconstructed surfaces, once we introduce correlation effects [47]. As each orbital is only one-quarter-filled per spin, the effect of the intrasite Coulomb interaction is to create a new peak, having 1/4 weight, located an energy U_{eff} above the original DOS. The metallic band reduces its weight per orbital from 1 to 3/4, and quarter of an electron per spin partially fills this band.

It is convenient to summarize our results for the 3×3 reconstruction and compare them with the $\sqrt{3} \times \sqrt{3}$ case. As regards the $\sqrt{3} \times \sqrt{3}$ surface, our discussion shows that this interface should present a metal–insulator transition (see figure 13) with an energy gap of around 1 eV for both the Sn/Ge(111) and the Sn/Si(111) cases. The 3×3 reconstruction retains, however, the same metallic character that LDA calculations show, although there is an important redistribution in the empty-state electron DOS as schematically shown in figure 15. The important point emerging from this discussion is that the difference in metallic properties between the two reconstructions can be used to confirm the validity of the dynamical fluctuations model presented above. The crucial point to notice is the following: if the $\sqrt{3} \times \sqrt{3}$ phase is a mixture of 3×3-like phases fluctuating among themselves, any technique probing

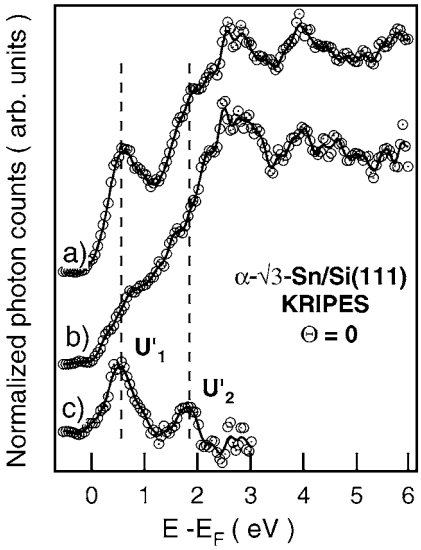

Figure 16. Normal-incidence ($\theta = 0°$) KRIPES spectra of Sn/Si(111)-α-$\sqrt{3}$ before (a) and after (b) exposure to roughly 1 L of atomic hydrogen. (c) The KRIPES difference between the spectra (a) and (b) (after [47]).

its possible insulator character will find a metallic interface. In contrast, if the $\sqrt{3} \times \sqrt{3}$ reconstruction had a static geometry with all the Sn atoms located at the same height above the surface, the system would present an insulator character. We conclude that *metallic character of the surface bands would be a fingerprint signalling the validity of the dynamical fluctuations model* [65].

Charrier *et al* [47] have explored this possibility, investigating the Sn/Si(111)-$\sqrt{3} \times \sqrt{3}$ interface [37]. The advantage of this system is that the defect-induced perturbation at RT has a much shorter spatial extent than in the Sn/Ge(111) interface. On the other hand, for the Sn/Si(111) interface no phase transition to the 3×3 reconstruction has yet been observed at LT [35, 68] (as our theoretical calculations predict); thus, analysing the metallic character of that interface would provide an independent confirmation of the validity of the dynamical fluctuations model [18] for this case, even if the 3×3 reconstruction is not stable at LT. In the study [47], angle-resolved inverse PES was used to explore the surface states above E_F. Figure 16 shows the KRIPES spectra for an incident angle $\theta = 0$, before and after deposition of roughly 1 L (langmuir) of activated hydrogen. The KRIPES difference curve clearly shows two peaks, U'_1 and U'_2, which can be associated with the Sn dangling-bond surface states. These results (see also [47]) clearly show that:

(a) there is a metallic band for the $\sqrt{3} \times \sqrt{3}$ reconstruction;

(b) a surface state appears around 1 eV above E_F, in correspondence with the upper correlated band shown in figure 15.

These results show the metallic character of the Sn/Si(111)-$\sqrt{3} \times \sqrt{3}$ reconstruction and afford an independent confirmation of the dynamical fluctuations model for that interface.

9. Summary and conclusions

This paper presents a critical review of our understanding of the reversible phase transition $\sqrt{3} \times \sqrt{3} \leftrightarrow 3 \times 3$ appearing for the α-phase of the Pb/Ge(111), Pb/Si(111), and Sn/Ge(111) interfaces. The Sn/Si(111) case is also discussed, although it apparently does not present the same phase transition. Our main discussion is presented for the Sn/Ge(111) and Sn/Si(111) cases, for which comprehensive theoretical calculations have been performed.

The experimental data and the theoretical analysis support the following conclusions:

(a) Sn/Ge(111) presents a reversible $\sqrt{3} \times \sqrt{3} \leftrightarrow 3 \times 3$ phase transition associated with a surface soft phonon. At LT, this soft mode freezes into the 3×3 reconstruction, while at RT the system vibrates with Sn adatoms displaying large vertical displacements; these dynamical fluctuations yield, on average, a $\sqrt{3} \times \sqrt{3}$ symmetry that retains locally a 3×3 reconstruction.
(b) The mechanism behind this phase transition is the electronic energy gain associated with the surface band splitting induced by the 3×3 reconstruction, that overcomes the elastic energy spent in the deformation of the system.
(c) Sn/Si(111) does not present a $\sqrt{3} \times \sqrt{3} \leftrightarrow 3 \times 3$ phase transition. Our calculations and the experimental evidence show, however, that the system can also be interpreted as presenting large vertical displacements within the dynamical fluctuations model found for Sn/Ge(111).
(d) Regarding the role of substitutional defects in Sn/Ge(111), we have found that although they can affect the transition temperature, they are not the driving force behind the $\sqrt{3} \times \sqrt{3} \leftrightarrow 3 \times 3$ phase transition. In particular, we find that the ordering of Ge substitutional defects at LT is induced by the ground state 3×3 reconstruction and not the other way around.
(e) Finally, we have shown that many-body effects introduce significant modifications in the LDOS of the Sn/Ge and Sn/Si(111) interfaces. In particular, we have found that a flat $\sqrt{3} \times \sqrt{3}$ reconstruction should present a Mott transition, while a 3×3 reconstruction is metallic. We conclude that the metallic character of the $\sqrt{3} \times \sqrt{3}$ interfaces affords an independent confirmation of the dynamical fluctuations model for both Sn/Ge(111) and Sn/Si(111).

To conclude, we should stress that these systems represent a good example of a new paradigm in surface science (that includes, among others, the Si(100)-2×1 case mentioned above and the Si–Ag $\sqrt{3} \times \sqrt{3}$ [69] system), where thermal fluctuations controlled by soft modes seem to explain the apparent contradiction between electronic properties and the structural symmetry observed.

Acknowledgments

We acknowledge financial support by the Spanish CICYT under contract MAT-2001-0665 and from Comunidad de Madrid (contract 07N/0050/2001).

References

[1] Le Lay G and Metois J J 1983 *Appl. Surf. Sci.* **17** 131
Metois J J and Le Lay G 1983 *Surf. Sci.* **133** 422
[2] Ichikawa T 1983 *Solid State Commun.* **17** 827
[3] Flores F and Tejedor C 1987 *J. Phys. C: Solid State Phys.* **20** 145

[4] Heslinga D R, Weitering H H, van der Werf D P, Klapwijk T M and Hibma T 1990 *Phys. Rev. Lett.* **64** 1589
[5] Le Lay G, Hricovini K and Bonnet J 1989 *Appl. Surf. Sci.* **41/42** 25
[6] See
Flores F, Ortega J and Pérez R 2002 *Survey of Semiconductor Physics: Electrons and other Particles in Semiconductors* vol 1, 2nd edn ed K Boer (New York: Wiley) p 63 ch 4
[7] Feidenhans'l R, Pedersen J S, Grey F and Johnson R L 1986 *Surf. Sci.* **178** 927
[8] Pedersen J S, Feidenhans'l R, Nielsen M, Kjaer K, Grey F and Johnson R L 1987 *Surf. Sci.* **189/190** 1047
[9] Carlisle J A, Miller T and Chiang T-C 1993 *Phys. Rev.* B **47** 3790
[10] Carlisle J A, Miller T and Chiang T-C 1993 *Phys. Rev.* B **47** 10 342
[11] Würde K, Krüger P, Mazur A and Pollmann J 1998 *Surf. Rev. Lett.* **5** 105
[12] Göthelid M, Björkqvist M, Grehk T M, Le Lay G and Karlsson U O 1995 *Phys. Rev.* B **52** R14 352
[13] Carpinelli J M, Weitering H H, Plummer E W and Stumpf R 1996 *Nature* **381** 398
[14] Carpinelli J M, Weitering H H, Bartkowiak M, Stumpf R and Plummer E W 1997 *Phys. Rev. Lett.* **79** 2859
[15] Custance O 2002 *PhD Thesis* Universidad Autonoma de Madrid
Custance O 2001 *Surf. Sci.* **482–5** 1399
[16] Charrier A 2001 *PhD Thesis* Université de Marseille-Luminy
[17] Goldoni A and Modesti S 1997 *Phys. Rev. Lett.* **79** 3266
[18] Ávila J, Mascaraque A, Michel E G, Asensio M C, Le Lay G, Ortega J, Pérez R and Flores F 1999 *Phys. Rev. Lett.* **82** 442
[19] Ortega J, Pérez R and Flores F 2000 *J. Phys.: Condens. Matter* **12** L21
[20] Pérez R, Ortega J and Flores F 2001 *Phys. Rev. Lett.* **86** 4891
[21] Ortega J, Pérez R, Jurczyszyn L and Flores F 2002 *J. Phys.: Condens. Matter* submitted
(Ortega J, Pérez R, Jurczyszyn L and Flores F 2001 *Preprint* cond-mat/0107121)
[22] Melechko A V, Braun J, Weitering H H and Plummer E W 2000 *Phys. Rev.* B **61** 2235
[23] Weitering H H, Carpinelli J M, Melechko A V, Zhang J, Bartkowiak M and Plummer E W 1999 *Science* **285** 2107
[24] Melechko A V, Braun J, Weitering H H and Plummer E W 1999 *Phys. Rev. Lett.* **83** 999
[25] Petersen L, Ismail and Plummer E W 2001 *Phys. Rev.* B **65** 020101
[26] Seehofer L, Falkenberg G and Johnson R L 1993 *Surf. Sci.* **290** 15
[27] Ancilotto F, Selloni A and Car R 1993 *Phys. Rev. Lett.* **61** 3685
[28] Baddorf A P, Jahns V, Zhang J, Carpinelli J M and Plummer E W 1998 *Phys. Rev.* B **57** 4579
[29] Zhang J, Ismail, Rous P J, Baddorf A P and Plummer E W 1999 *Phys. Rev.* B **60** 2860
[30] Mascaraque A, Ávila J, Álvarez J, Asensio M C, Ferrer S and Michel E G 1999 *Phys. Rev. Lett.* **82** 2524
[31] Bunk O, Zeysing J H, Falkenberg G, Johnson R L, Nielsen M, Nielsen M M and Feidenhans'l R 1999 *Phys. Rev. Lett.* **83** 2226
[32] Floreano L, Petaccia L, Benes M, Cvetko D, Goldoni A, Gotter R, Grill L, Morgante A, Verdini A and Modesti S 1999 *Surf. Rev. Lett.* **6** 1091
[33] Petaccia L, Floreano L, Benes M, Cvetko D, Goldoni A, Grill L, Morgante A, Verdini A and Modesti S 2001 *Phys. Rev.* B **63** 115406
[34] Petaccia L, Floreano L, Goldoni A, Cvetko D, Morgante A, Grill L, Verdini A, Comelli G, Paolucci G and Modesti S 2001 *Phys. Rev.* B **64** 193410
[35] Uhrberg R I G *et al* 2000 *Phys. Rev.* B **62** 8082
[36] Ottaviano L, Crivellari M, Lozzi L and Santucci S 2000 *Surf. Sci.* **445** L41
[37] Charrier A, Pérez R, Thibaudau F, Debever J-M, Ortega J, Flores F and Themlin J-M 2001 *Phys. Rev.* B **64** 115407
[38] Yamanaka T and Ino S 2000 *Phys. Rev.* B **61** R5074
[39] Horikoshi K, Tong X, Nagao T and Hasegawa S 1999 *Phys. Rev.* B **60** 13 287
[40] Le Lay G, Ariston V Yu, Bostrom O, Layet J M, Asensio M C, Ávila J, Huttel Y and Cricenti A 1998 *Appl. Surf. Sci.* **123–4** 440
[41] Uhrberg R I G and Balasubramanian T 1998 *Phys. Rev. Lett.* **81** 2108
[42] Kidd T E, Miller T and Chiang T-C 1999 *Phys. Rev. Lett.* **83** 2789
[43] Uhrberg R I G, Zhang H M and Balasubramanian T 2000 *Phys. Rev. Lett.* **85** 1036
[44] Le Lay G, Goshtasbi Rad M, Göthelid M, Karlsson U O, Ávila J and Asensio M C 2001 *Appl. Surf. Sci.* **175–6** 201
[45] Goldoni A, Cepek C and Modesti S 1997 *Phys. Rev.* B **55** 4109
[46] Mascaraque A, Ávila J, Michel E G and Asensio M C 1998 *Phys. Rev.* B **57** 14 758
[47] Charrier A, Pérez R, Thibaudau F, Debever J-M, Ortega J, Flores F and Themlin J-M 2001 *J. Phys.: Condens. Matter* **13** L521

[48] Petaccia L, Grill L, Zangrando M and Modesti S 1999 *Phys. Rev. Lett.* **82** 386
[49] Mascaraque A 2000 *PhD Thesis* Universidad Autonoma de Madrid
[50] Ávila *et al* J 2000 *Appl. Surf. Sci.* **162–3** 48
[51] Floreano L, Cvetko D, Bavdek G, Benes M and Morgante A 2001 *Phys. Rev.* B **64** 075405
[52] Cvetko D, Floreano L, Crottini A, Morgante A and Tommasini F 2000 *Surf. Sci.* **447** L147
[53] Inoue K, Morikawa Y, Terakura K and Nakayama M 1994 *Phys. Rev.* B **49** 14 774
[54] Nakamura Y, Kawai H and Nakayama M 1997 *Phys. Rev.* B **55** 10 549
[55] Kidd *et al* T E 2000 *Phys. Rev. Lett.* **85** 3684
[56] Demkov A A, Ortega J, Sankey O F and Grumbach M P 1995 *Phys. Rev.* B **52** 1618
Sankey O F and Niklewski D J 1989 *Phys. Rev.* B **40** 3979
[57] Clarke L J, Stich I and Payne M C 1992 *Comput. Phys. Commun.* **72** 14
[58] de Gironcoli S, Scandalo S, Ballabio G, Santoro G and Tosatti E 2000 *Surf. Sci.* **454–6** 172
[59] Jurczyszyn L, Ortega J, Pérez R and Flores F 2001 *Surf. Sci.* **482–5** 1350–4
[60] Ávila J, Mascaraque A, Le Lay G, Michel E G, Göthelid M, Ascolani H, Álvarez J, Ferrer S and Asensio M C 2001 *Preprint* cond-mat/0104259
[61] Bruce A D and Cowley R A 1980 *Adv. Phys.* **29** 219
[62] Ballabio G, Scandalo S and Tosatti E 2000 *Phys. Rev.* B **61** 13 345
[63] Jemander S T *et al* 2001 *Surf. Sci.* **475** 181
[64] Flores F, Ortega J and Pérez R 1999 *Surf. Rev. Lett.* **6** 411
[65] Flores F, Ortega J, Pérez R, Charrier A, Thibaudau F, Debever J-M and Themlin J-M 2001 *Prog. Surf. Sci.* **67** 299
[66] Pou P *et al* 2000 *Phys. Rev.* B **62** 4309
[67] Pankratov O and Scheffler M 1993 *Phys. Rev. Lett.* **70** 351
[68] Ottaviano L *et al* 2000 *Surf. Sci.* **464** 57
[69] Sasaki N, Watanabe S and Tsukada M 2002 *Phys. Rev. Lett.* **88** 046106